

Second-order photonic topological insulator with corner states


Bi-Ye Xie,¹ Hong-Fei Wang,¹ Hai-Xiao Wang,² Xue-Yi Zhu,¹ Jian-Hua Jiang,^{2,*} Ming-Hui Lu,^{1,3,4,†} and Yan-Feng Chen¹

¹*National Laboratory of Solid State Microstructures and Department of Materials Science and Engineering, Nanjing University, Nanjing 210093, China*

²*School of Physical Science and Technology, and Collaborative Innovation Center of Suzhou Nano Science and Technology, Soochow University, 1 Shizi Street, Suzhou 215006, China*

³*Jiangsu Key Laboratory of Artificial Functional Materials, Nanjing University, Nanjing 210093, China*

⁴*Collaborative Innovation Center of Advanced Microstructures, Nanjing University, Nanjing 210093, China*

 (Received 19 May 2018; revised manuscript received 16 October 2018; published 26 November 2018)

Higher-order topological insulators (HOTIs) which go beyond the description of conventional bulk-boundary correspondence, broaden the understanding of topological insulating phases. Being mainly focused on electronic materials, HOTIs have not yet been found in photonic crystals. Here, we propose a type of two-dimensional second-order photonic crystals with zero-dimensional corner states and one-dimensional boundary states for optical frequencies. All of these states are topologically nontrivial and can be understood based on the theory of topological polarization. Moreover, by tuning the easily fabricated structure of the photonic crystals, different topological phases can be realized straightforwardly. Our study can be generalized to higher dimensions and provides a platform for higher-order photonic topological insulators and semimetals.

DOI: [10.1103/PhysRevB.98.205147](https://doi.org/10.1103/PhysRevB.98.205147)

I. INTRODUCTION

Topological insulators (TIs) and topological semimetals (TSMs) have been theoretically and experimentally studied due to their distinct edge states and transport properties [1,2]. Normally, d -dimensional (d D) TIs have d D gapped bulk states and $(d-1)$ D gapless boundary states. Recently, the concept of higher-order topological insulators (HOTIs) has been put forward to describe those topological insulators (TIs) which have lower-dimensional gapless boundary states [3–8]. Generally speaking, a d D TI with $(d-1)$ D, $(d-2)$ D, ..., $(d-n-1)$ D gapped boundary states and $(d-n)$ D gapless boundary states is called an n th-order TI. The HOTIs broaden the family of nontrivial topological insulating phases. Moreover, the HOTIs have unique boundary states which go beyond the conventional bulk-boundary correspondence and are characterized by novel topological invariants [3,4,6,8].

However, it is not easy to realize these topological phases in electronic materials. One of the obstacles is that the Fermi levels of electronic materials are not always in the topologically nontrivial band gaps or at the gapless points. The band structures of photonic crystals (PCs) provide us with platforms to study various topological phases such as photonic topological insulators (PTIs) and photonic topological semimetals (PTSMs) without limitations imposed by the Fermi level [9–34]. In terms of the HOTIs, the topological corner and hinge states in PCs can be used to design robust optical cavities and waveguides. So far, the observations of HOTIs are only realized in mechanical metamaterials [35], electrical circuits [36,37], and weakly coupled

optical waveguides [38] which are described predominantly with quadrupole or rotation-symmetry-protected topological orders. The extension of the notion of HOTIs to PCs without negative coupling is still lacking.

In this paper, we propose a two-dimensional (2D) PTI which is the 2D photonic generalization of the Su-Schrieffer-Heeger (SSH) model [39]. Similarly to the 1D SSH model, the topological classes of the 2D photonic SSH model can be determined by different lattice structures as proposed in Ref. [40]. Previous studies of the 2D photonic SSH model are focused on the zero Berry curvature of the bulk band topology and gapless 1D edge states [40,41]. Here, by a theoretical investigation and numerical simulation, we demonstrate that there are coexisting edge and corner states when two topologically distinct PCs are placed together to form box-shaped boundaries. We reveal that both the bulk polarization, described by the vector $\mathbf{P} = (P_x, P_y)$, and the edge polarization, $p_x^{v_y}$ and $p_y^{v_x}$, are quantized by the mirror symmetries $M_x := x \rightarrow -x$ and $M_y := y \rightarrow -y$. The theoretical predictions and analysis are supported by numerical simulations for all-dielectric PCs at optical frequencies.

This paper is organized as follows. The band structures of PC and topological corner states are introduced in Sec. II. In Sec. III, we study the 1D edge states and extend our discussion from isotropic case to anisotropic case where the lattice constant may be different for the x and y directions. Finally, a summary is given in Sec. IV.

II. SECOND-ORDER TOPOLOGICAL PHOTONIC CRYSTALS

We consider a 2D PC with mirror symmetries as shown in Fig. 1(a). There are four identical dielectric rods in each unit cell which form isotropic ($l_x = l_y$) or anisotropic (with

*joejhjiang@hotmail.com

†luminghui@nju.edu.cn

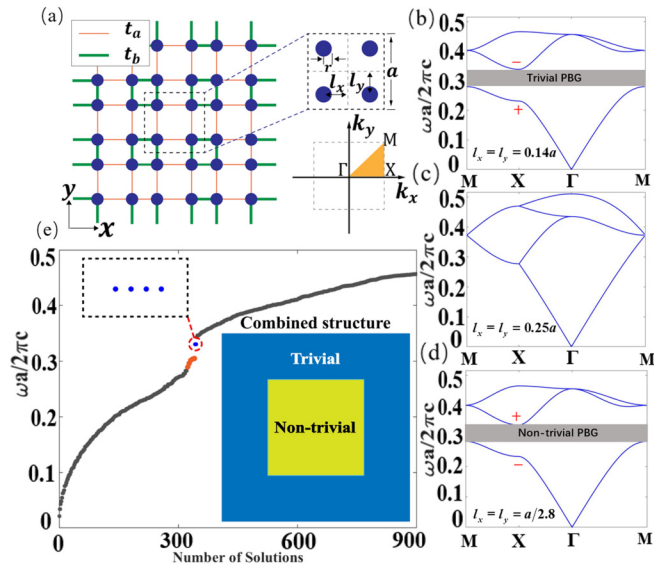


FIG. 1. (a) The 2D photonic SSH model and the first Brillouin zone. We set $a = 1.5 \mu\text{m}$, $r = 0.12a$, and the relative dielectric constant $\epsilon = 12$ for all the cases. The coupling strength is denoted as t_a and t_b . (b)–(d) The band inversion induced by changing l . + (–) indicates the even (odd) parity of the band. (b) $l = 0.14a$ (topologically trivial PBG). (c) $l = 0.25a$ (band-gap closing). (d) $l = a/2.8$ (topologically nontrivial PBG). We choose the values of l in order to make a maximal overlap between the band gaps in (b) and (d). (e) Photonic eigenmodes of a combined structure where the PC in (d) is inside a box and the PC in (b) is outside the box, as shown in the inset. There are four degenerate states localized at the four corners in the band gap. Here, edge (bulk) modes are denoted by orange (gray) points, whereas the corner modes are represented by blue points.

$l_x \neq l_y$) PCs, depending on their configurations (square or rectangular). The center of the configuration is at the center of the unit cell which is also the origin of the coordinates throughout this paper. For a 2D PC, the dielectric function is homogeneous along the z direction and therefore has a reflection symmetry. Consequently, the electromagnetic fields which are the eigenmodes of the PC can be classified into transverse-electric (TE) fields and transverse-magnetic (TM) fields. Without loss of generality, here we consider the TM modes throughout this paper and the TE modes can be studied in a similar way.

Photonic band structures of distinct topological properties can be realized by tuning the distance between the four rods. Despite such a simple design, topological edge and corner states [see Fig. 1(e)] can appear in the photonic band gap (PBG) between the first and the second bulk bands (denoted as PBG I). For isotropic PCs with $l_x = l_y \equiv l$, we find that the intra- and inter-unit-cell distances (l_{intra} and l_{inter}) between the neighboring rods control the band topology. Here, $l_{\text{intra}} = 2l$ and $l_{\text{inter}} = a - 2l$, where a is the lattice constant. For $l_{\text{intra}} < l_{\text{inter}}$ the PBG I has trivial topology, whereas for $l_{\text{intra}} > l_{\text{inter}}$ the PBG I carries nontrivial topology as signified by the parity inversion at the X point. The parities of the bands which are the eigenvalues of the inversion symmetry operator are defined in the same way as those in Ref. [40]. A transition

appears at $l_{\text{intra}} = l_{\text{inter}}$ (i.e., $l = a/4$), where the PBG is closed by the band degeneracy on the Brillouin zone boundary lines (e.g., the MX line) [see Figs. 1(b)–1(d)].

The photonic band structure and the topological properties of the isotropic PC can be well approximated by the tight-binding model as depicted in Fig. 1(a), whose Hamiltonian is

$$\mathcal{H}(\mathbf{k}) = \begin{pmatrix} 0 & h_{12} & h_{13} & 0 \\ h_{12}^* & 0 & 0 & h_{24} \\ h_{13}^* & 0 & 0 & h_{34} \\ 0 & h_{24}^* & h_{34}^* & 0 \end{pmatrix}. \quad (1)$$

Here, $h_{12} = t_a + t_b \exp(ik_x)$, $h_{13} = t_a + t_b \exp(-ik_y)$, $h_{24} = t_a + t_b \exp(-ik_y)$, $h_{34} = t_a + t_b \exp(ik_x)$, and $\mathbf{k} = (k_x, k_y)$.

The tight-binding parameters t_a, t_b reflect the intra- and inter-unit-cell couplings between the neighboring rods, respectively. Here, we neglect the higher-order couplings such as the next-nearest-neighbor coupling. This approximation is valid for lower-band structure and this validity is verified by the numerical calculation of the band structures of PC as shown in Figs. 1(b)–1(d) which is similar to the band structure calculated by directly diagonalizing tight-binding Hamiltonian as shown in Ref. [40]. It is known that the above tight-binding model has nontrivial topology as characterized by the 2D polarization \mathbf{P} where

$$P_i = -\frac{1}{(2\pi)^2} \int d^2\mathbf{k} \text{Tr}[\hat{A}_i], \quad i = x, y, \quad (2)$$

where $(\hat{A}_i)_{mn}(\mathbf{k}) = i \langle u_m(\mathbf{k}) | \partial_{k_i} | u_n(\mathbf{k}) \rangle$, where m, n run over all occupied bands, and $|u_m(\mathbf{k})\rangle$ is the periodic Bloch function for the m th band. The 2D polarization is connected to the 2D Zak phase [40] via $\theta_i = 2\pi P_i$ for $i = x, y$. The 2D Zak phase of the PC equals (π, π) [i.e., $\mathbf{P} = (\frac{1}{2}, \frac{1}{2})$] for $t_a < t_b$ (i.e., $l_{\text{intra}} > l_{\text{inter}}$) and reveals that the PC is in the topological nontrivial insulating phase, while it equals $(0, 0)$ for $t_a > t_b$ (i.e., $l_{\text{intra}} < l_{\text{inter}}$) where the PC is in the trivial insulating phase. Beyond the isotropic tight-binding model, P_x and P_y can be different, resulting in nontrivial topological invariants $\mathbf{P} = (\frac{1}{2}, 0)$ or $\mathbf{P} = (0, \frac{1}{2})$, beside $\mathbf{P} = (\frac{1}{2}, \frac{1}{2})$. We will show that only the last case can lead to both topological edge and corner states, whereas the first two cases can only support topological edge states but not corner states.

Consider a box-shaped boundary between the PC with $\mathbf{P} = (\frac{1}{2}, \frac{1}{2})$ and the PC with $\mathbf{P} = (0, 0)$ [see Fig. 1(e)]. There are boundaries along the x and y directions which support topological edge states due to the 2D Zak phase. For instance, the nontrivial Zak phase $\theta_x = \pi$ for each k_y gives rise to the edge states on the boundaries along the y direction for the whole edge Brillouin zone $k_y \in [-\frac{\pi}{a}, \frac{\pi}{a}]$. A similar bulk-edge correspondence works for the boundaries along the x direction. We consider a ribbon structure where a strip of a nontrivial PC is sandwiched in between two PCs in the trivial phase. Then the band structure for the ribbon, namely, the projected band structure, contains the information of the lower-dimensional edge states. We numerically simulated this structure and the dispersion of the 1D edge state is clearly shown in Fig. 2. For the isotropic case, the projected band structures for the k_x and k_y directions are the same due to the symmetry. Without loss of generality, we calculate

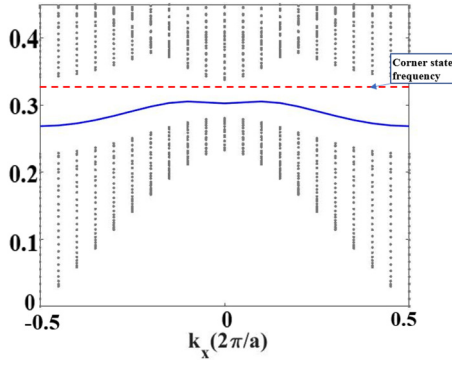


FIG. 2. Projected band structure along the k_x direction for Fig. 1(e) (isotropic). There are 1D edge states appearing in the first band gap which are topologically protected by bulk polarization as depicted by the solid blue line. The dashed red line labels the frequency of the corner states.

the projected band structure along the k_x direction for the combined structure as shown in Fig. 1(e). The result shows that there are 1D edge states in the first band gap. We also label the frequency of one of the corner states as the dashed line in Fig. 2.

Remarkably, those 1D edge states themselves are similar to the 1D photonic SSH model with nontrivial topology protected by M_x (M_y) for the edges along the x (y) direction. The topology of the edge states is characterized by the edge polarizations, $p_y^{v_x}$ and $p_x^{v_y}$, for edges perpendicular to the x and y directions, respectively.

The topological theory of polarization [3,6] connects the polarization of the edge states to the eigenvalues of the nested Wilson loops (mathematical details are given in the Supplemental Material [42]). In simple terms, the nested Wilson loops construct the Zak phases of the edge states by projecting the bulk Bloch states into a sector which is topologically equivalent to the edge states using the Wannier band bases, $|w_{x,\alpha}(\mathbf{k})\rangle = \sum_{n \in \mathcal{N}_{\text{PBG}}} v_n^\alpha(k_y) |u_n(\mathbf{k})\rangle$. Here, $n \in \mathcal{N}_{\text{PBG}}$ stands for summation over all bands below the PBG, and $v_n^\alpha(k_y)$ is the α th Wilson-loop eigenvector for the Wilson-loop operator with k_x looping from $-\pi/a$ to π/a at fixed k_y . With the nested Bloch states, one can calculate the polarization for the edge states perpendicular to the x direction,

$$p_y^{v_x} = -\frac{1}{(2\pi)^2} \int d^2\mathbf{k} \text{Tr}[\hat{\mathcal{B}}_y], \quad (3)$$

where $(\hat{\mathcal{B}}_y)_{\alpha,\beta} = i \langle w_{x,\alpha}(\mathbf{k}) | \partial_{k_y} | w_{x,\beta}(\mathbf{k}) \rangle$. Remarkably, for the PBG considered in this work, there is only one photonic band below the PBG. Hence, there is only one Wilson-loop eigenvalue and the eigenvector $v_1^1(k_y) \equiv 1$. Hence, the nested Wilson loop becomes the same as the bulk Wilson loop. However, the above equation is valid only when there are physical edge states on the boundary perpendicular to the x direction, i.e., only when $P_x = \frac{1}{2}$ (the edge polarization should vanish when $P_x = 0$). Putting these two factors together, we find that $p_y^{v_x} = (2P_x) \times P_y = \frac{1}{2}$. Similarly, $p_x^{v_y} = (2P_y) \times P_x = \frac{1}{2}$. Numerical calculations of these topological indices are presented in the Supplemental Material [42].

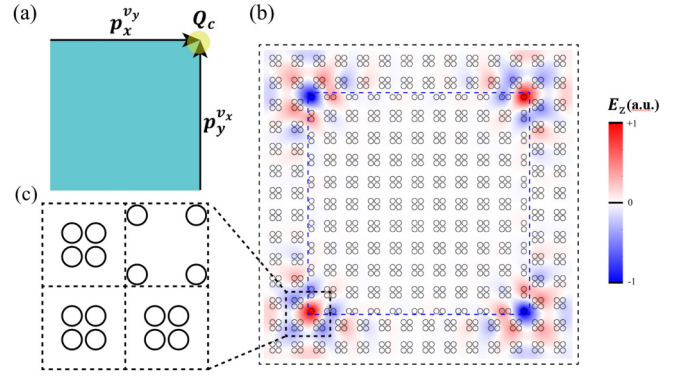


FIG. 3. (a) Schematic of bulk-edge-corner correspondence. The nontrivial topology of the bulk (cyan region) leads to the emergence of the edge states, while the polarization of the edge (indicated by the black arrows) results in the formation of the topological corner state (indicated by the shallow yellow region). (b) There are in total four degenerate corner states at the four corners with frequency 66.0 THz. The electrical fields E_z (a.u. stands for arbitrary units) are strongly localized at the corners (a superposition of the four degenerate corner states is shown here). The blue dashed line indicates the boundary between the two PCs. (c) The zoom-in structure of the corner, where the dashed black lines indicate the border of the unit cells. The topological unit cell has a much larger l ($l = a/2.8$) compared to the three trivial unit cells ($l = 0.14a$).

The topological edge states along the x and y directions meet at the corner of the box-shaped combined structure shown in Figs. 1(e) and 3(b) where the outside PC has trivial topology, i.e., $\mathbf{P} = (0, 0)$. Differing from Refs. [3,35–37], there is no quadrupole topological order in our system, since there is only a single band below the PBG. Therefore, the topological corner charge is determined by the edge polarizations as [6]

$$Q_c = p_x^{v_y} + p_y^{v_x} = 4P_x P_y. \quad (4)$$

If the inner PC has $\mathbf{P} = (\frac{1}{2}, \frac{1}{2})$, then $Q_c = 1$. This quantized corner charge gives rise to a single corner state in each of the four corners, as confirmed by the numerical simulation in Fig. 3(b). The detailed dielectric structure of the combined structure is given in Fig. 3(c) for one of the corners. The spectrum of the eigenmodes is already shown in Fig. 1(e) where four degenerate corner modes are found in the PBG. The electromagnetic fields of the corner modes are strongly localized at each of the four corners. These corner states are protected by the nontrivial topology, as characterized by $Q_c = 1$, as well as the mirror symmetries M_x and M_y which quantize the polarizations. The bulk-edge-corner correspondence elucidated above shows the topological protection in a hierarchy of dimensions, which is a smoking-gun signature of HOTIs. The robustness of the corner states against perturbations is demonstrated by the simulations presented in the Supplemental Material [42].

On the other hand, the emergence of the corner modes can be understood from the tight-binding model, particularly when one considers the extreme case where $t_a = 0$ and $t_b \neq 0$. In this case, the four corner sites of the tight-binding model become “dangling atoms” which trap zero-energy corner

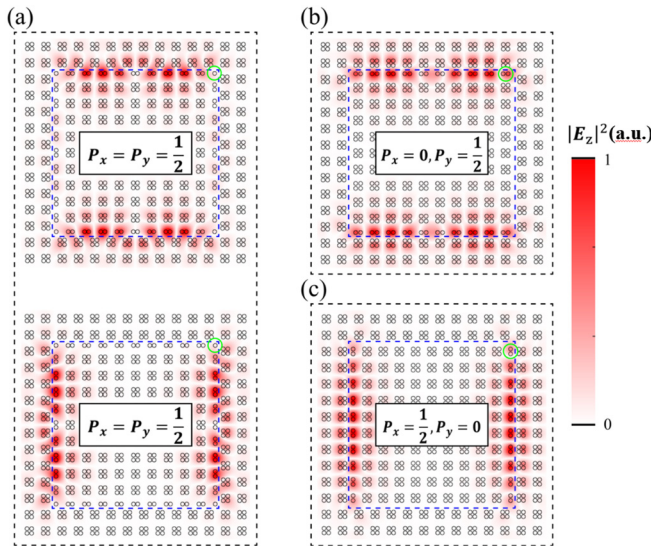


FIG. 4. Anisotropic 2D photonic SSH model where $l_x \neq l_y$. The PCs have the same a , r , and ϵ as the isotropic 2D photonic SSH model but have deformed lattice structures characterized by l_x and l_y . The eigenstates are solved by COMSOL. For the outer PC, we set $l_x = l_y = 0.14a$. For inner PCs, we set (a) $l_x = 0.37a$ and $l_y = 0.35a$. Nontrivial phase in both x and y directions. Two sets of degenerate edge states (DESS) with different frequencies. For the DESS in the upper (lower) figure, the frequency is 60.2 THz (61.1 THz). (b) $l_x = 0.15a$ and $l_y = 0.35a$. The x direction in the topologically trivial phase and the y direction in the topologically nontrivial phase. There are only 1D DESS in the upper and lower sides. The frequency is 64.2 THz. (c) $l_x = 0.35a$ and $l_y = 0.15a$. The x direction in the topologically nontrivial phase and the y direction in the topologically trivial phase. There are only 1D DESS in the left and right sides. The frequency of the state in this figure is 65.2 THz. The solid green circles emphasize the differences in the corner structures and field strengths in (a)–(c). The dashed blue lines label the boundaries of two PCs.

modes. Since the band structure of this extreme case can be adiabatically connected to the $t_a \neq 0$ case, they are in the same topological class and the corner states will always exist as long as $|t_a| < |t_b|$. In terms of the topological invariants, $Q_c = 1$ corresponds to the $\mathbf{P} = (\frac{1}{2}, \frac{1}{2})$ phase.

III. ANISOTROPIC PHOTONIC CRYSTALS AND TOPOLOGICAL PHASE DIAGRAM

Next, we extend our discussions to anisotropic 2D PCs where $l_x \neq l_y$ as shown in Fig. 4. The bulk polarizations are determined by the intra- and inter-unit-cell distance between the rods along the x and y directions, l_{intra}^i and l_{inter}^i with $i = x, y$. For instance, $l_{\text{intra}}^x > l_{\text{inter}}^x$ leads to nontrivial topological indices $P_x = \frac{1}{2}$. The edge polarizations are given by $p_x^{\text{vx}} = 2P_x P_y$.

For a box-shaped combined structure with the outer PC of $\mathbf{P} = (0, 0)$, the edge states along the y (x) direction emerge when the inner PC has $P_x = \frac{1}{2}$ ($P_y = \frac{1}{2}$), as shown in Fig. 4. The electrical fields for the edge states in Fig. 4(a) indicate that the four dielectric rods at the corners have vanishing field intensity, emerging as dangling atoms in the topological

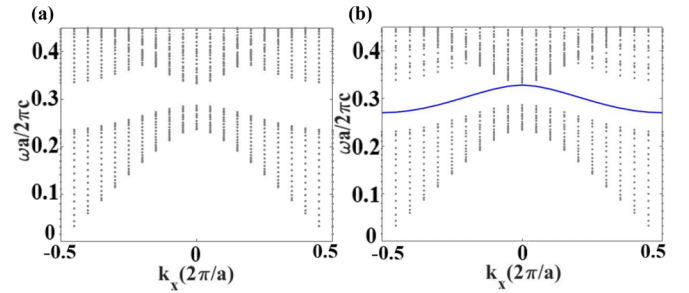


FIG. 5. Projected band structures for Fig. 4(c) along the k_x and k_y direction as shown in (a) and (b), respectively. (a) There are no 1D edge states along the k_x direction. (b) There are 1D edge states in the band gap along the k_y direction as depicted by the solid blue line.

SSH model. Such unoccupied dielectric rods leave space for unpaired topological corner modes. In comparison, for inner PCs of $\mathbf{P} = (\frac{1}{2}, 0)$ or $(0, \frac{1}{2})$ as shown in Figs. 4(b) and 4(c), the corner rods have finite field intensities and do not support corner modes. These observations are consistent with the corner charge given in Eq. (4). We also study the 1D edge states in the anisotropic cases. For the anisotropic case, namely, with the x direction in the topological nontrivial phase and the y direction in the topological trivial phase, the projected band structures are different for the k_x and k_y directions. We calculate the projected band structures for Fig. 4(c) as a demonstration. The result is shown in Figs. 5(a) and 5(b) for the projected band structures along the k_x and k_y

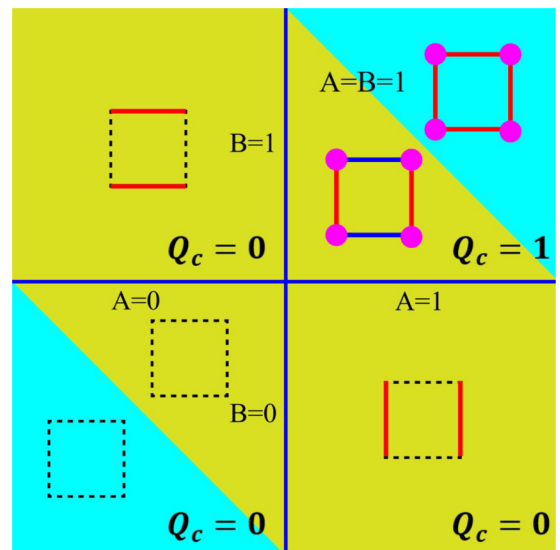


FIG. 6. Classification of all kinds of the generalized 2D photonic SSH model with different configurations in the x and y directions. A (B) = 1 means the 2D photonic SSH model is in the topologically nontrivial phase along the x (y) direction. A (B) = 0 means the 2D photonic SSH model is in the topologically trivial phase along the x (y) direction. The blue area represents isotropic cases and the yellow area represents anisotropic cases. The dashed lines represent there are no 1D edge states and solid lines represent the existence of 1D edge states. The solid circles mean there are corner states. The edge (or corner) states of the same color have the same frequency, whereas the states with different colors have different frequencies.

directions, respectively. The results of the simulation match our theoretical predictions well.

According to the above discussions, the whole phase diagram of the 2D PCs can be classified into four different phases, as depicted in Fig. 6: the topologically trivial phase with $l_{\text{intra}}^i < l_{\text{inter}}^i$ for both $i = x$ and y of which $\mathbf{P} = (0, 0)$ and $Q_c = 0$; the two phases with nontrivial bulk topology but zero corner charge, i.e., $\mathbf{P} = (\frac{1}{2}, 0)$ or $(0, \frac{1}{2})$, and $Q_c = 0$ where $l_{\text{intra}}^x < l_{\text{inter}}^x$ or $l_{\text{intra}}^y < l_{\text{inter}}^y$; and the phase with both nontrivial bulk topology and corner charge, i.e., $\mathbf{P} = (\frac{1}{2}, \frac{1}{2})$ and $Q_c = 1$ where $l_{\text{intra}}^i > l_{\text{inter}}^i$ for both $i = x$ and y . Therefore, by simply changing the relative distances of the nearest rods in the anisotropic 2D photonic SSH model, we can achieve various topological phases with different 1D DESs as well as corner states. This can be potentially used to design different optical topological switches for photonic integrated chips in the future.

IV. CONCLUSIONS AND DISCUSSIONS

We propose a simple realization of the second-order topological insulator in all-dielectric photonic crystals (PCs) with corner states. The exotic corner states can be regarded as the 0D boundary states of the 1D edge of the 2D PC which is topologically protected by mirror symmetries. Besides, we study the anisotropic 2D photonic SSH model and find that the 1D DESs arise due to the 1D structures existing in the 2D photonic SSH model. By adjusting the distances between the nearby rods in the x and y directions, the emergence of the edge and corner states can be controlled straightforwardly.

These topologically protected edge and corner states may be valuable for robust waveguides, optical couplers,

and optical topological circuit switches. Our PC can be experimentally realized in a surface plasmon polariton (SPP) slab and in microwave frequencies. In both cases, the structure is similar to our model but has a finite size in the z direction. The relevant parameters need to be modified from our theoretical model but the topological properties are the same.

If our theory is generalized to a 3D photonic SSH model, there can be second-order and third-order topological insulating phases where topological hinge states and corner states can emerge, respectively. The 3D second-order topological semimetals may be achieved by stacking the 2D photonic SSH model along the z direction. The 3D second-order topological semimetals have rich bulk and boundary properties which are yet to be explored [43].

Note added. Recently, we became aware of a paper showing 0D topological bound states in a 2D PC due to the presence of dislocation (a topological defect) [44], demonstrating another mechanism for lower-dimensional topological light trapping.

ACKNOWLEDGMENTS

B.-Y.X., H.-F.W., X.-Y.Z., M.-H.L., and Y.-F.C. are supported by the National Key R&D Program of China (Grants No. 2018YFA0306200, No. 2017YFA0303700) and the National Nature Science Foundation of China (Grant No. 11625418), as well as the Academic Program Development of Jiangsu Higher Education (PAPD). H.-X.W. and J.-H.J. are thankful for support from the National Natural Science Foundation of China (Grant No. 11675116).

-
- [1] M. Z. Hasan and C. L. Kane, *Rev. Mod. Phys.* **82**, 3045 (2010).
 - [2] X. L. Qi and S. C. Zhang, *Rev. Mod. Phys.* **83**, 1057 (2011).
 - [3] W. A. Benalcazar, B. A. Bernevig, and T. L. Hughes, *Science* **357**, 61 (2017).
 - [4] Z. Song, Z. Fang, and C. Fang, *Phys. Rev. Lett.* **119**, 246402 (2017).
 - [5] J. Langbehn, Y. Peng, L. Trifunovic, F. von Oppen, and P. W. Brouwer, *Phys. Rev. Lett.* **119**, 246401 (2017).
 - [6] W. A. Benalcazar, B. A. Bernevig, and T. L. Hughes, *Phys. Rev. B* **96**, 245115 (2017).
 - [7] F. Schindler, A. M. Cook, M. G. Vergniory, Z. Wang, S. S. P. Parkin, B. A. Bernevig, and T. Neupert, *Sci. Adv.* **4**, eaat0346 (2018).
 - [8] M. Ezawa, *Phys. Rev. Lett.* **120**, 026801 (2018).
 - [9] F. D. M. Haldane and S. Raghu, *Phys. Rev. Lett.* **100**, 013904 (2008).
 - [10] Z. Wang, Y. Chong, J. D. Joannopoulos, and M. Soljačić, *Nature (London)* **461**, 772 (2009).
 - [11] M. Hafezi, E. A. Demler, M. D. Lukin, and J. M. Taylor, *Nat. Phys.* **7**, 907 (2011).
 - [12] Y. Poo, R. X. Wu, Z. Lin, Y. Yang, and C. T. Chan, *Phys. Rev. Lett.* **106**, 093903 (2011).
 - [13] A. B. Khanikaev, S. H. Mousavi, W. K. Tse, M. Kargarian, A. H. MacDonald, and G. Shvets, *Nat. Mater.* **12**, 233 (2013).
 - [14] M. Hafezi, S. Mittal, J. Fan, A. Migdall, and J. M. Taylor, *Nat. Photonics* **7**, 1001 (2013).
 - [15] M. C. Rechtsman, J. M. Zeuner, Y. Plotnik, Y. Lumer, D. Podolsky, F. Dreisow, S. Nolte, M. Segev, and A. Szameit, *Nature (London)* **496**, 196 (2013).
 - [16] L. Lu, J. D. Joannopoulos, and M. Soljačić, *Nat. Photonics* **8**, 821 (2014).
 - [17] W. J. Chen, S. J. Jiang, X. D. Chen, B. Zhu, L. Zhou, J. W. Dong, and C. T. Chan, *Nat. Commun.* **5**, 5782 (2014).
 - [18] S. A. Skirlo, L. Lu, and M. Soljačić, *Phys. Rev. Lett.* **113**, 113904 (2014).
 - [19] W. Gao, M. Lawrence, B. Yang, F. Liu, F. Fang, B. Beri, J. Li, and S. Zhang, *Phys. Rev. Lett.* **114**, 037402 (2015).
 - [20] L. H. Wu and X. Hu, *Phys. Rev. Lett.* **114**, 223901 (2015).
 - [21] T. Ma, A. B. Khanikaev, S. H. Mousavi, and G. Shvets, *Phys. Rev. Lett.* **114**, 127401 (2015).
 - [22] C. He, X. C. Sun, X. P. Liu, M. H. Lu, Y. Chen, L. Feng, and Y. F. Chen, *Proc. Natl. Acad. Sci. U.S.A.* **113**, 4924 (2016).
 - [23] D. Leykam, M. C. Rechtsman, and Y. D. Chong, *Phys. Rev. Lett.* **117**, 013902 (2016).
 - [24] F. Gao, Z. Gao, X. Shi, Z. Yang, X. Lin, H. Xu, J. D. Joannopoulos, M. Soljačić, H. Chen, L. Lu, and Y. Chong, *Nat. Commun.* **7**, 11619 (2016).

- [25] L. Xu, H. X. Wang, Y. D. Xu, H. Y. Chen, and J. H. Jiang, *Opt. Express* **24**, 18059 (2016).
- [26] X. C. Sun, C. He, X. P. Liu, M. H. Lu, S. N. Zhu, and Y. F. Chen, *Prog. Quantum Electron.* **55**, 52 (2017).
- [27] X. Zhu, H. X. Wang, C. Xu, Y. Lai, J. H. Jiang, and S. John, *Phys. Rev. B* **97**, 085148 (2018).
- [28] Y. Yang, Y. F. Xu, T. Xu, H. X. Wang, J. H. Jiang, X. Hu, and Z. H. Hang, *Phys. Rev. Lett.* **120**, 217401 (2018).
- [29] L. Lu, L. Fu, J. D. Joannopoulos, and M. Soljačić, *Nat. Photonics* **7**, 294 (2013).
- [30] L. Lu, Z. Wang, D. Ye, L. Ran, L. Fu, J. D. Joannopoulos, and M. Soljačić, *Science* **349**, 622 (2015).
- [31] H. X. Wang, L. Xu, H. Y. Chen, and J. H. Jiang, *Phys. Rev. B* **93**, 235155 (2016).
- [32] M. Xiao, Q. Lin, and S. Fan, *Phys. Rev. Lett.* **117**, 057401 (2016).
- [33] H. X. Wang, Y. Chen, Z. H. Hang, H. Y. Kee, and J. H. Jiang, *npj Quantum Mater.* **2**, 54 (2017).
- [34] B. Yang, Q. Guo, B. Tremain, R. Liu, L. E. Barr, Q. Yan, W. Gao, H. Liu, Y. Xiang, J. Chen, and C. Fang, *Science* **359**, 1013 (2018).
- [35] M. Serra-Garcia, V. Peri, R. Susstrunk, O. R. Bilal, T. Larsen, L. G. Villanueva, and S. D. Huber, *Nature (London)* **555**, 342 (2018).
- [36] C. W. Peterson, W. A. Benalcazar, T. L. Hughes, and G. Bahl, *Nature (London)* **555**, 346 (2018).
- [37] S. Imhof, C. Stefan, F. Bayer, J. Brehm, L. Molenkamp, T. Kiessling, F. Schindler, C. H. Lee, M. Greiter, T. Neupert, and R. Thomale, *Nat. Phys.* **14**, 925 (2018).
- [38] J. Noh, W. A. Benalcazar, S. Huang, M. J. Collins, K. Chen, T. L. Hughes, and M. C. Rechestman, *Nat. Photonics* **12**, 408 (2018).
- [39] W. P. Su, J. R. Schrieffer, and A. J. Heeger, *Phys. Rev. Lett.* **42**, 1698 (1979).
- [40] F. Liu and K. Wakabayashi, *Phys. Rev. Lett.* **118**, 076803 (2017).
- [41] F. Liu, H. Y. Deng, and K. Wakabayashi, *Phys. Rev. B* **97**, 035442 (2018).
- [42] See Supplemental Material at <http://link.aps.org/supplemental/10.1103/PhysRevB.98.205147> for details on the topological theory of polarization which connects the polarization of the edge states to the eigenvalues of the nested Wilson loops, numerical calculations of the polarization for the edge states, and simulations on topological protections of corner states against perturbations.
- [43] M. Lin and T. L. Hughes, [arXiv:1708.08457](https://arxiv.org/abs/1708.08457).
- [44] F. F. Li, H. X. Wang, Z. Xiong, Q. Lou, P. Chen, R. X. Wu, Y. Poo, J. H. Jiang, and S. John, *Nat. Commun.* **9**, 2462 (2018).